



## Indomethacin Delivery from PCL Nanofibrous Scaffolds Enhances Biomineralization and Cell Adhesion: Biocompatible Scaffold Model for Teeth Regeneration

Sara A.M. El-Sayed<sup>a\*</sup>, Mostafa Mabrouk<sup>a</sup>, Ahmed R. Wassel<sup>b</sup>, Mahmoud T. Abo-Elfadl<sup>c, d</sup>  
Bothaina M Abdel-Hady<sup>e</sup> and Hanan H. Beherei<sup>a\*</sup>



<sup>a</sup>*Refractories, Ceramics and Building Materials Department, National Research Centre, 33El Bohouth St. (former EL Tahrir St.), Dokki, PO Box 12622, Giza, Egypt.*

<sup>b</sup>*Electron Microscope and Thin Film Department, Physics Research Division, National Research Centre, 33El Bohouth St. (former EL Tahrir St.), Dokki, PO Box 12622, Giza, Egypt.*

<sup>c</sup>*Biochemistry Department, Biotechnology Research Institute, National Research Centre, 33El Bohouth St. (former EL Tahrir St.), Dokki, PO Box 12622, Giza, Egypt.*

<sup>d</sup>*Cancer Biology and Genetics Laboratory, Centre of Excellence for Advanced Sciences, National Research Centre, 33El Bohouth St. (former EL Tahrir St.), Dokki, PO Box 12622, Giza, Egypt.*

<sup>e</sup>*Polymer division, National Research Centre, 33El Bohouth St. (former EL Tahrir St.), Dokki, PO Box 12622, Giza, Egypt.*

### Abstract

3D porous scaffolds have shown remarkable promise in the fields of tissue regeneration and medication delivery. This study focuses on constructing uniform 3D structures from polycaprolactone (PCL) loaded with nano-bioactive glass (58S) for the purpose of facilitating the development of dental cells. The scaffold surfaces were activated using chitosan, a biocompatible compound. The scaffolds underwent thorough characterization, encompassing the assessment of their physicochemical properties, thermal behavior, and microstructural aspects. A study was conducted on the release of the anti-inflammatory drug indomethacin, and the mode of cell death was evaluated using MG-63 cell lines. Human Dental Pulp Stem Cells (HDPSCs) were specifically planted into the scaffolds made of nanofibers. Scanning electron microscopy (SEM) investigation demonstrated significant cell adhesion, multiplication, and expansion. The scaffolds containing 58S exhibited markedly larger densities of mineralized nodules produced by HDPSCs, suggesting enhanced mineralization and the possibility of enhanced regeneration of tooth tissue. The results revealed that the scaffolds contained 58S (NF6) and the scaffolds that contained the drug into the nanofibers matrix (NF7) had a slower release rate (9%) than the scaffolds that contained the drug through the coated layer (NF4) which was 16%. Moreover, the cell viability illustrated that (NF4), (NF6) and (NF7) are the best samples which recorded more than 300%, 100% and 200% viability percent, respectively. These novel 3D homogenous scaffolds show significant potential for precise drug administration and the restoration of dental tissues, leading to revolutionary progress in dental healthcare.

**Keywords:** Homogenous porous scaffold; Surface modification; Controlled indomethacin delivery; Dental tissue regeneration

### 1. Introduction

Bone diseases are being one of the most common diseases due to ageing, bad lifestyle, or trauma. Recently, construction of three-dimensional (3D) scaffolds has attracted great interest in bone tissue engineering. Electrospinning technology has unique advantages in the construction of 3D micro pore structures and can engender perpetual fibers with varying diameters, ranging from nano- to microscale [1–5]. Electrospinning method is the technique that allows obtaining micro- and nanofibers based on a high voltage applied during the electrospinning process. This high voltage enhances the viscous solution which controlled by a syringe to draw and collected on a collector plate as fibers. There are many factors that affect the characteristics of the produced fibers such as: surface tension, molecular weight, viscosity, solvent, solution conductivity [6, 7].

The electrospun nanofibers look like the microstructure of the extracellular matrix (ECM) and can give a rich microenvironment to the development of cells, minerals deposition, and the recovery of tissue [8]. Electrospun nanofiber

\*Corresponding author e-mail: [sarali\\_87@yahoo.com](mailto:sarali_87@yahoo.com); (Sara A.M. El-Sayed).

Receive Date: 24 July 2024, Revise Date: 15 August 2024, Accept Date: 25 August 2024

DOI: 10.21608/ejchem.2024.306910.10076

©2025 National Information and Documentation Center (NIDOC)

scaffolds have been extensively applied in optoelectronics, catalysis, sensor technology, medication delivery and tissue engineering owing to their high specific surface area, porosity, and diverse surface functionality [9, 10].

Nevertheless, classical electrospun nanofibers are coming out in random orientation of two-dimensional (2D) membranes, which limits their uses in 3D regeneration. Up till now, four techniques for manufacturing 3D nanofiber scaffolds were recorded: post-treatment of the 2D electrospun nanofibers (sintering, shirring, and mechanical treatment) [11, 12], multilayer electrospinning by spinning time prolongation or utilizing a subsidiary electric field [13, 14], template receiver [15, 16], and self-assembly of the nanofibers [17, 18]. Scaffolds which were fabricated for bone tissue engineering should be acquired some properties: biocompatible, non-toxic, bioactive (the ability of formation of new bone), their ability to induce the cell to differentiate for bone repair and growth, in addition to pore structure that allows the exchange of nutrients, oxygen and waste products [19]. One of the common used polymers for electrospinning technique is polycaprolactone PCL (synthetic polymer), and this comes back due to its mechanical and biocompatibility properties which important for biomedical applications [6].

Although successful 3D scaffolds can be achieved utilizing the previous advantages, some limitations still observed. For instance, wide distances between adjacent nanofiber layers, minimal productivity, complicated methods, random self-assembly, and poor mechanical properties [20–25]. Therefore, effective fabrication of 3D nanofiber scaffolds with micro and macro pores is a challenge for electrospinning. In addition, the importance of presence of inorganic phase into the polymer matrix should be taken into consideration [26–29]. Bioactive glass nanoparticles (58S), which possesses good bioactivity, osteoinductivity and osteoconductivity was chosen to be the inorganic filler of the fabricated scaffolds. Moreover, surface activation of the synthetic nanofibers using polysaccharide material such as chitosan was reported for enhancement the biomineralization and biocompatibility [30, 31]. Chitosan is a natural polymer which has gained a great deal of attention due to its superior properties such as: biocompatibility, biodegradability, nontoxicity and drug-loading capacity [6]. It is used for bone tissue engineering because it has osteogenic properties and chemical properties which similar to glycosaminoglycans of ECM [32].

In addition, indomethacin was used as one type of small molecular drugs [33–35], which has considerable advantages in directing the differentiation of the cells that used for tissue regeneration and function repair. That may be attributed to their precise and controllable induction effect on cells.

The aim of this study to provide a new strategy to design and fabricate of 3D micro composite nanofiber scaffold for dental regeneration in addition to enhance the sustained indomethacin release. We used stainless steel meshes as the receiver instead of the traditional plate, and obtained patterned nanofiber meshes by methanol/chloroform solution were screened to form 3D PCL porous nanofiber structures with micro and macro hierarchical pores. To fulfill the target of this research, several techniques were employed to investigate the effect of chitosan coating, 58S and indomethacin existence on the final features of the obtained scaffolds. These techniques include DSC, SEM, FTIR and BET surface area measurements. Moreover, medication delivery was determined in PBS along with ions release and the pH changes of the soaking environment. Furthermore, cell compatibility and biomineralization were assessed by SEM. Finally, the cell death mode (MG-63 cell line) was also evaluated.

## 2. Experimental section

### 2.1. Materials

The PCL pellets (MWt=80,000 g/mol), HPLC chloroform and Indomethacin (>99%), were purchased from Sigma-Aldrich (USA). Nano bioactive glass (58S) was prepared as mentioned previously in our research [36]. Methanol was purchased from Aladdin (China). Glacial Acetic Acid (99%, MWt=60.05 g/mol, ADWIC, El=Nasr pharmaceutical chemicals, Egypt). Chitosan (deacetylation degree 75%), (MWt=100,000–300,000 g/mol; ACROS Organics, Germany).

### 2.2. Sample preparation

#### 2.2.1. Preparation of 3D PCL nanofiber scaffolds

The polymer nanofibers scaffold was prepared by dissolving 7.5% PCL polymer (0.3 g) into (4 ml) co-solvent of methanol and chloroform (1:3). Then, the mixture was loaded into a syringe pump of the electro-spinner under the following electrospinning condition (distance between the tip and the collector: 10 cm, tip thickness: 0.90 x 70 mm BL/LB (20G\*2 3/4<sup>n</sup>), the applied voltage: 20 KV and the collector was covered with the stainless steel mesh), to acquire the designed nanofiber scaffold, stainless steel mesh (304) was cut to produce small pieces of mesh, cleaned through ultrasonication and utilized as the extraordinary recipient for electrospinning.

#### 2.2.2. Preparation of 3D PCL/ 58S bioactive glass composite nanofiber scaffolds

The composite nanofibers scaffold was prepared by loading the PCL polymer solution (demonstrated above) with 40% 58S nanoparticles  $w/w$  (0.12 g) for 1 h using magnetic stirrer at room temperature. Afterwards, the pump syringe of the electrospinner was filled with the mixture under the electrospinning conditions (distance between the tip and the collector: 10 cm, tip thickness: 1.20 x 40 mm BC/SB (18G\*1 1/2<sup>n</sup>), the applied voltage: 20 KV; collector was coated with the stainless steel mesh). The achieved composite scaffolds were compared with pure PCL nanofiber scaffolds. Furthermore, preparation of

PCL/indomethacin nanofibers was obtained by dispersion of 30%  $w/w$  indomethacin (0.1 g) into the PCL pure solution under the previous composite electrospinning conditions.

### 2.2.3. Chitosan surface modifications of nanofiber scaffolds

PCL/58S, PCL/indomethacin composite nanofiber scaffolds and pure PCL nanofibers were dip coated in 2% indomethacin-free chitosan solution and indomethacin containing chitosan solution with weight ratio of (7:3). The coating solution was obtained through dissolving chitosan (2 g) in (100 ml) of acidified distilled water at room temperature. Afterwards, indomethacin (0.3 g) was dispersed in the chitosan solution [37]. The coated nanofiber scaffolds were allowed to dry overnight at room temperature and symbolized as shown in table 1.

## 2.3. Characterization

### 2.3.1. Thermal analysis

In order to study the effect of coating of chitosan along with the presence of 58S on the thermal behaviour of the nanofiber scaffolds, Thermogravimetric Analysis (TGA) and Differential Scanning Calorimetric (DSC) were performed. Particularly, 10 mg of the nanofiber was placed in a crucible of platinum under the air firing regime, range of temperature was 50–700 °C and firing rate of 5 °Cmin<sup>-1</sup>, using (SDT Q600 V20.9Build 20) (TA, USA) instrument. The results were compared using aluminium oxide powder as a reference.

### 2.3.2. Microstructure of the 3D porous nanofiber scaffolds

The microstructure of the 3D porous nanofiber scaffolds was examined by scanning electron microscope (JEOL JXA-840A, Electron probe micro analyzer, Tokyo, Japan) at 15 kV. The 3D nanofibers scaffolds were coated with gold to become electrically conductive before imaging by gold-sputter coating (SPI Module TMS putter Coater, SPI Supplies, and PA) and were placed onto the SEM stub utilizing carbon tape.

### 2.3.3. FTIR analysis

To examine the influence of the coating of the chitosan on the chemical integrity of the nanofiber scaffolds, infrared spectra was obtained using Fourier Transformer Infrared spectrophotometer (ATR-FTIR) (model FT/IR-6100 type A, Jasco, International, Tokyo, Japan). Each spectrum was measured at a wavenumber of 4000–400 cm<sup>-1</sup>.

### 2.3.4. Surface Area measurements

By using an automatic analyzer (Quanta chrome Nova Automated Gas Sorption System Version 1.12, USA) the specific surface area and pore-size distribution were determined. Brunauer–Emmett–Teller (BET) method was applied. At 77 K through indirect molecular adsorption methods like nonlocal density functional theory (NLDFT) and N<sub>2</sub> isotherms microscopic pore-size distribution was performed.

### 2.3.5. *In vitro* indomethacin evaluations

The *in vitro* release of indomethacin from the nanofiber scaffolds was conducted in Phosphate Buffer Saline (PBS) at 37 °C in an incubator for distinctive intervals of time (1, 3, 7, 14 and 28 days). The nanofiber scaffolds were soaked in plastic containers filled with 100 ml of PBS. Withdrawn of 5 ml from these containers was collected after each period and replaced by fresh PBS to evaluate the indomethacin release along with the concentrations of the leached ions from the soaked samples into PBS. All experiments were performed on triplicates of the fabricated nanofiber scaffolds. Indomethacin released amount into the solution was measured using UV spectrophotometer at a wavelength of 330 nm [30]. The indomethacin loading and encapsulation efficiency were calculated according to the following Equations.

$$\% \text{ Drug loading} = \frac{\text{Weight of drug in formulation}}{\text{Weight of total formulation}} \times 100 \quad (1)$$

$$\% \text{ Encapsulation Efficiency} = \frac{\text{Actual drug loading}}{\text{Theoretical drug loading}} \times 100 \quad (2)$$

Moreover, the variations in the PBS ions' concentrations (Ca and P elements) by a chemical kit using UV/visible spectrometer (model, SP-2000UV, Tokyo, Japan) at a wavelength of 585 and 640 nm respectively. All experiments were performed on triplicates of the fabricated nanofiber scaffolds. The evaluation of the Ca and P ions' concentrations has important investigation for biomineralization. The nanofiber scaffolds were removed from the PBS, further washed with ethanol and dried, then weighed to assess their mass loss (degradation). The initial weight of the nanofibers scaffold was noted as  $W_0$  and the dry weight after immersion time as  $W_i$  and the degradation of nanofibers was calculated using Equation 3.

$$\text{Degradation \%} = \frac{(W_0 - W_t)}{W_0} \times 100 \quad (3)$$

**Table 1. The codes of the prepared nanofiber scaffolds**

Sample name	Code
Pure PCL nanofibers	NF1
Composite PCL/58S nanofibers	NF2
PCL nanofibers coated with indomethacin free chitosan	NF3
PCL nanofibers coated with chitosan containing indomethacin	NF4
PCL/58S nanofibers coated with indomethacin-free chitosan	NF5
PCL/58S nanofibers coated with chitosan containing indomethacin	NF6
PCL/Indomethacin nanofibers coated with indomethacin-free chitosan	NF7

### 3.6. Mechanism of indomethacin release

Korsmeyer–Peppas model was utilized to determine the release kinetics of indomethacin from the homogenous composite scaffolds. The Korsmeyer–Peppas model is given as:

$$M_t/M_\infty = Kt^n \quad (4)$$

At time  $t$  the fraction released drug is  $M_t/M_\infty$ , release exponent is  $n$  and  $K$  rate constant. The value is  $n < 0.5$  when profiles of release follow quasi-Fickian diffusion, but if  $n = 0.5$ , it follows Fickian diffusion and if  $n = 0.5 - 1.0$ , it follows anomalous transport or non-Fickian.

#### 2.3.7. *In vitro* assessments

##### 2.3.7.1. Cell seeding on scaffolds

Primary HDPSCs were isolated from sound third molar indicated for extraction in a healthy adult patient after approval by the Medical Research Ethics Committee (MREC) of National Research Centre (NRC), Egypt (Approval No. **16/340**). Based on broadly settled protocols, HDPSC isolation was conducted [38]. Cells were suspended at a density of  $5 \times 10^6$  cells/ml, with a total volume of 100  $\mu$ l per scaffold. In brief, 9.5 mm diameter, 4 mm height scaffolds were prehydrated in PBS for 15 min and put in six well-plates. The cell suspension was then added to the scaffolds, 50  $\mu$ l on one side of each scaffold, and incubated for 15 min in a 5% CO<sub>2</sub>, 37 °C incubator and allowed initial attachment. Scaffolds were subsequently turned over and the procedure repeated. After the second incubation period, 5 ml of supplemented Dulbecco's modified Eagle's medium growth medium was added to each well and precultured for 7 days (medium change on day 3) [38].

##### 2.3.7.2. SEM of cells with scaffolds

Using SEM (JEOL JXA-840A, Electron probe micro analyzer, Tokyo, Japan) at 15 kV, seeded scaffolds were imaged after 3 and 21 days of culture to investigate the influence of the coating of chitosan on the cell attachments. In details, the cell morphology of cells culture after 3 and 21 days was examined on the prepared scaffolds by washing three times with PBS buffer and once with distilled water. After that, the cells were fixed on the scaffold surface by using 4% glutaraldehyde and dehydrated in a graded ethanol solution (20, 30, 40, 50, 70, and 95% ethanol) each for 10–20 min. Samples with cells were attached to stubs and coated with an ultra-thin layer of gold in a coating apparatus, and then the morphology of cells was observed by SEM.

#### 2.3.8. Cytocompatibility of the synthesized materials

Human bone osteosarcoma (MG-63) was purchased from ATCC, USA. DMEM (Dulbecco's Modified Eagle's Medium) was the routinely cultured medium. The medium was supplemented with 10% fetal bovine serum (FBS), 2 mM L-glutamine, containing 100 units/ml penicillin G sodium, 100 units/ml streptomycin sulphate, and 250 ng/ml amphotericin B. All the previous materials were from Lonza, (Basel, Switzerland). At subconfluency at 37 °C in humidified air containing 5% CO<sub>2</sub>, the cells were maintained. At 37 °C monolayer cells were harvested after trypsin/EDTA treatment for sub-culturing. All measurements are recorded three times. All biological studies conducted in this research work were approved by the Medical Research Ethics Committee (MREC) of National Research Centre (NRC), Egypt (Approval No. **095082023**). All methods were performed in accordance with all the regulations set forth in International Council for Harmonisation of Technical Requirements for Pharmaceuticals for Human Use - Good Clinical Practice (**ICH-GCP**) and the local committee guidelines.

##### 2.3.8.1. Mode of cell death

Equal slices of the tested samples were added to cultured cells. The used 8 well cell culture plates were purchased from (SPL, Seoul, South Korea) at density  $10^4$  cells / well. The mode of the cell death was investigated after 24 and 72 h of incubation

after staining with acridine orange (100  $\mu\text{g}/\text{mL}$ ) and ethidium bromide (100  $\mu\text{g}/\text{mL}$ ) dual stain dissolved in phosphate buffer saline (PBS) at equal volume, all obtained from Merck KGaA (Darmstadt, Germany). After cells staining, the cells were investigated under the fluorescent microscope (AxioImager Z2, Zeiss, Jena, Germany). The live cells appeared as a green color, the early apoptotic, late apoptotic or necrotic cells appeared as yellow, orange, or red colors, respectively [39]. The measurements were performed three times.

### 2.3.8.2. MTT cytotoxicity

To evaluate the cytotoxicity of the tested samples on the MG-63 cell line, MTT (3-[4, 5-dimethylthiazole-2-yl]-2, 5-diphenyltetrazolium bromide) that was purchased from Merck KGaA (Darmstadt, Germany) was used. This method based on conversion of tetrazolium rings of the yellow MTT to dark blue insoluble formazan crystals by the active mitochondrial dehydrogenase enzyme of living cells. Therefore, if the liberation of dark blue color (result

## 3. Results and discussion

### 3.1. Thermal analysis

DSC results of chitosan coated scaffolds (NF3 and NF5) are shown in Fig. 1a with reference to (NF1 and NF2) scaffolds. The glass transition temperatures of NF1, NF3, NF2 and NF5 were noted as endothermic peaks at 382.04, 225.16, 331.67 and 265.84  $^{\circ}\text{C}$ , respectively. Their exothermic peaks attributed to the crystallization temperatures were detected at 417.78, 412.5, 354.27 and 399.12  $^{\circ}\text{C}$ , respectively. DSC test showed single exothermic peaks at 417.78  $^{\circ}\text{C}$  and 354.27  $^{\circ}\text{C}$ , in case of NF1 and NF2, respectively, which are corresponding to the thermal decomposition of PCL [41, 42]. It is noticed that the crystallization temperatures are slightly changed after coating the nanofibers scaffolds (NF3 and NF5) by chitosan polymer where chitosan has an exothermic peak at approximately 300  $^{\circ}\text{C}$  that result in shifting of the NF1 exothermic peak. TGA results Fig. 1b showed the difference between NF1 and NF2 scaffolds and their coated forms, only mass decomposition was observed for non-coated scaffolds around 400  $^{\circ}\text{C}$  assigned to PCL decomposition. While, the decomposition of 58S was not detected for NF2 scaffold as the firing range was below its melting temperature. In case of the chitosan coated scaffolds they have demonstrated two mass decompositions one attributed to chitosan with 20-30% of the total mass around 350  $^{\circ}\text{C}$ , followed by mass loss up to 80-90% around 450  $^{\circ}\text{C}$ , which is assigned to degradation of PCL. The above observations confirmed the presence of organic continents of the scaffolds (PCL and chitosan), and also highlighted the positive influence of chitosan coating on the thermal stability of the scaffolds based on the shift of PCL decomposition from 400 to 450  $^{\circ}\text{C}$ . Close results were achieved for previous PCL membranes coated with  $\beta$ -cyclodextrin and PVA layers [37].

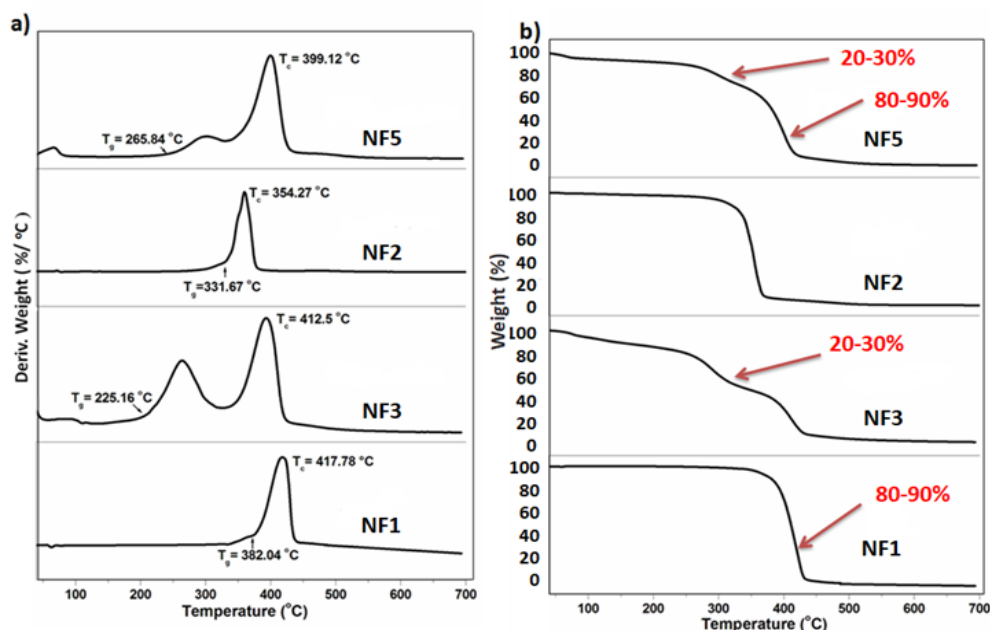


Figure 1. a) DSC and b) TGA curves of NF1, NF2, NF3 and NF5 nanofibers scaffolds

### 3.2. Microstructural properties

The influence of 58S on the morphology of the obtained scaffolds was monitored utilizing SEM as shown in Fig. 2. It is noticed for NF1 scaffold (Fig. 2 (a, b)) that it consisted of multilayer structure like meshes nanofibers. They possess thicker and smoother pore walls, which illustrate the ribs of the nanofiber meshes and the region between the adjacent pore walls is relatively thin. On the other hand, NF2 scaffold (Fig. 2 (c, d)) demonstrates rough

fibers surface compared to NF1 fibers. This difference in nanofibers surface is corresponding to the presence of 58S. However, both of them (NF1 and NF2) demonstrate a good constructing substrate for 3D structure. These microstructures were consistent with the reported research work by Song et al., 2017 [43]. In addition to that, it is obvious that the nanofibers diameter ranging from 300–1500 nm and randomly arranged that allows interconnections between pores.

Moreover, the surface modifications of the scaffolds coated with chitosan were recorded also using SEM as represented in Fig. 3. It is clear that the surface modification had the same effect on both 3D scaffolds NF3 and NF5 that shown in Fig. 3 (a, b), respectively as they demonstrate the same bulky nature. This could be explained according to the known characteristic for the dipping technique used in the current research, which guarantee a homogeneous distribution and infiltration for the chitosan within the 3D scaffolds and on the top of their surfaces, the same morphology was reported by Mabrouk et al., 2018 [37] for tramadol-loaded PCL ribbons coated with  $\beta$ -cyclodextrin and PVA using the dipping technique.

### 3.3. FTIR analysis

In order to assure the existence of chitosan coating on the scaffolds' surfaces and their influence on chemical integrity of the prepared NF1 and NF2, FTIR analyses were conducted (Fig. 4). The NF1 (Pure PCL) spectrum possessed two characteristic bands at 2942 and 2865  $\text{cm}^{-1}$  that were corresponding to stretching C–H. Another band was detected at 1725  $\text{cm}^{-1}$  that was corresponding to C=O. Two specific bands to PCL were noted at 1365 and 1168  $\text{cm}^{-1}$ , which are corresponding to deformation  $\text{CH}_2$  [44]. On the other hand, chitosan indomethacin-free coated nanofibers (NF3 and NF5) possessed many characteristic bands as illustrated in Fig.4. Band observed at 3745  $\text{cm}^{-1}$  was corresponding to the –OH. NF1 bands at 2942, 2865  $\text{cm}^{-1}$  were shifted at 3019, 2877  $\text{cm}^{-1}$  due to presence of chitosan (presence of – $\text{CH}_3$  group at 3000  $\text{cm}^{-1}$ ) and the same shift was noted also for NF2. In addition, bands recorded at 1533 and 1403  $\text{cm}^{-1}$  (NF3); 1542 (NF5) were attributed to the N–H primary amide group of vibrations of –OH group of the primary alcoholic group, respectively, which affirm the presence of chitosan. Bands at 1313 and 1687  $\text{cm}^{-1}$  (NF5) were corresponding to the stretching of C–O–N and C=O groups, respectively [45]. The bands at 1014 (NF3) and 1020  $\text{cm}^{-1}$  (NF5) are related to the glycoside bonding that confirms the existence of chitosan as well [46].

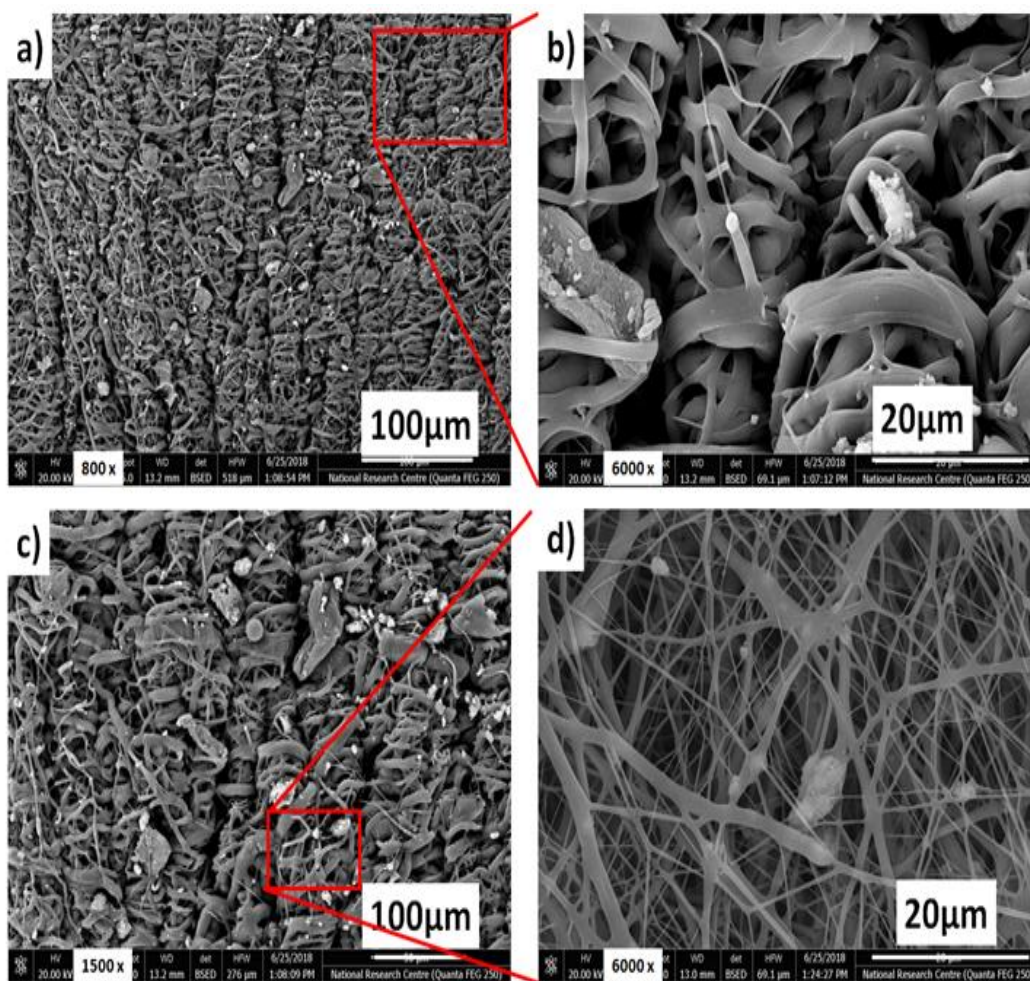


Figure 2. presents the microstructure study of NF1 and NF2 using scanning electron microscopy (SEM). Panels a) and b) show NF1 at two different magnifications (100, and 20  $\mu\text{m}$ ), while panels c) and d) show NF2 at two different magnifications (100, and 20  $\mu\text{m}$ )

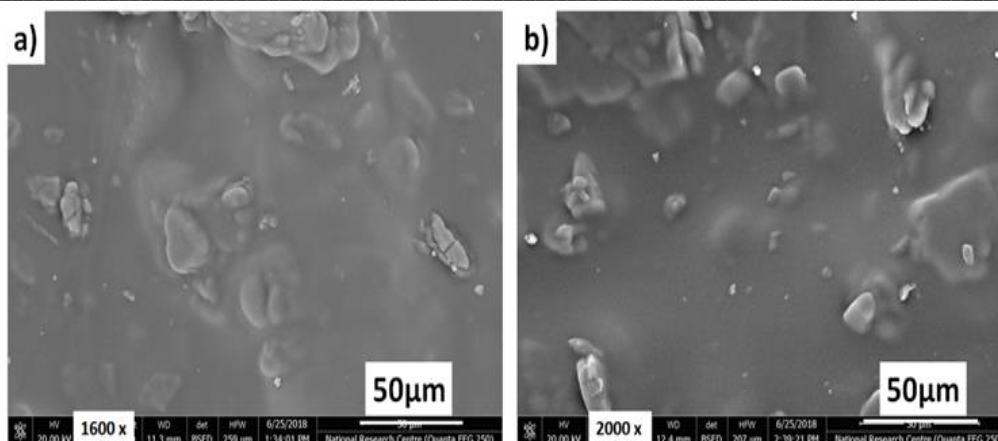


Figure 3. depicts the application of chitosan coating, the surface modification of the generated nanofiber scaffolds a) NF3 and b) NF5 by the scanning electron microscope (SEM)

### 3.4. Surface Area measurements

Surface area parameters were evaluated for chitosan coated and chitosan-free scaffolds using BET surface area to figure out the difference between the two groups and this was summarized in Table 2. It can be noted that, scaffold NF1 possess the lowest BET surface area (NF1= 0.902 m<sup>2</sup>/g) compared to indomethacin-free chitosan coated (NF5= 3.214 m<sup>2</sup>/g), PCL loaded with 58S nanofibers scaffold (NF2= 10.334 m<sup>2</sup>/g) and the highest surface area was recorded for pure PCL scaffold coated with indomethacin-free chitosan (NF3= 68.153 m<sup>2</sup>/g). This indicates that infiltration of 58S within the nanofibers matrix or chitosan surface modifications enhance the surface area of the obtained scaffolds and these results are attributed to the fact that the nanosize increase the surface area [47] and the chitosan has a large surface area [48]. On the other hand, remarkable decrements were observed for the main pore diameter of pure PCL nanofibers (NF1= 389.900 nm) in the presence of 58S particles along with chitosan coatings for scaffolds NF2, NF3 and NF5 as

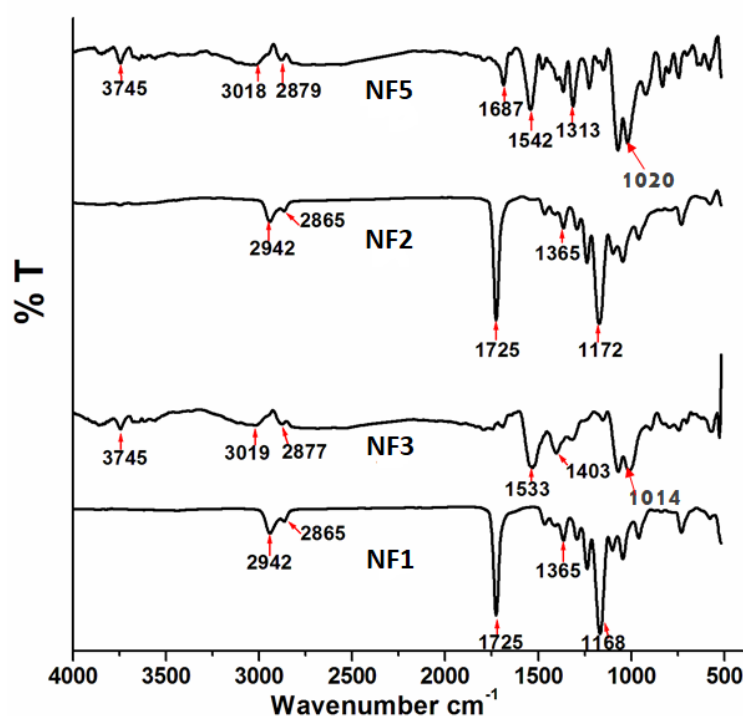


Figure 4. Demonstrates FTIR spectra of the fabricated nanofiber scaffolds before and after surface modification

they demonstrated mean pore diameters of 9.912, 9.234 and 2.999 nm, respectively. Moreover, the means of pore volumes were also slightly changed in the presence of 58S and chitosan coatings as could be noted from Table 2. These measurements imply that the microstructure parameters of the current nanofibers scaffolds are to be adjusted by controlling the presence of filler as well as surface modifications. Early conducted researches confirmed the superiority of scaffolds with adjustable microstructures over the non-controlled ones in augmentation of bone defects [49-51].

### 3.5. *In vitro* indomethacin evaluations

#### 3.5.1. Changes of PBS ions' concentrations

In order to investigate the effect of coating and/or 58S on the indomethacin release and their effective role; NF4, NF6 and NF7 scaffolds were prepared. In addition, investigation what is the effect of the presence of the indomethacin drug inside the scaffold matrix and outside through the coating layer. The variation of PBS ions' concentrations through the study time intervals (1, 3, 7, 14 and 28 days) are correlated to absorption and precipitation of PBS ions on the nanofibers surface or dissolution of 58S ions into the PBS medium as shown in Fig. 5. P ion concentrations demonstrated in Fig. 5a, which revealed that in the beginning the concentration of P ion recorded the higher value as it is one of the main components of PBS solution. With increasing the submersion time (3 days) water uptake increased owed to presence of chitosan coating, which results in decreasing of P concentration in the PBS solution. After 7 days of immersion, absorbed ions were dissolved again into PBS solution that caused increasing of P ions along with dissolution of ions from 58S. However, at the time range between 14 and 28 days the P ions returned to steady state due to concentration stability as the nanofiber scaffolds reached water uptake saturation stage. In case of Ca ion (Fig. 5b) the lowest values were noted in the beginning as PBS solution does not contain Ca ion. Afterwards, the Ca ion concentration increased, especially for scaffolds loaded with 58S.

**Table 2. Parameters of the surface area of the developed scaffolds**

Samples	BET Surface (m <sup>2</sup> /g)	Mean Pore volume (cm <sup>3</sup> /g)	Mean Pore diameter (nm)
NF1	0.902	0.088	389.900
NF2	10.334	0.031	9.912
NF3	68.153	0.157	9.234
NF5	3.214	0.024	2.999

It was also noted that the time range between 14 and 28 days Ca ion concentrations reached to steady state as the nanofibers scaffolds reached water uptake saturation stage. Moreover, the PBS pH changes during the time intervals were recorded as illustrated in Fig. 5c. The changes in pH of the PBS showed little change during the whole test. The variation of pH for NF5 come bake to containing 58S in the coating layer without drug. The release of 58S ions (P and Ca) caused this variation in pH values. In details, the drop of pH value is corresponding to P release because of the acidic nature of P ion. Afterwards, pH back up again because Ca is alkaline metal. The pH range was from 7.4 (start pH) to 7.65 (final pH) that is relatively neutral and in the same line of our early research [45]. The changes of the PBS ions concentration results and the pH values confirmed that the nanofibers scaffolds reach the steady state in the period of 14 and 28 days of soaking in PBS.

#### 3.5.2. *In vitro* degradation studies

The mass loss (%) of the nanofiber scaffolds was investigated by applying the degradation study in PBS solution at the same time intervals (1, 3, 7, 14 and 28 days). It was noted that the mass loss (%) of the scaffolds was between 3 to 28 % after 7 days for NF4 (Fig. 5d). Scaffolds that didn't contain 58S (NF3 and NF4) lost their mass more than the other scaffolds (NF5 and NF6) due to 58S existence increases the attachment of chitosan on the nanofibers surface and decrease their degradation rate. Adjusting the degradation rate using coatings of polysaccharides (chitosan) is more favorable for long-term reformation of damaged site in bone regeneration as has been confirmed by previous researches focused on fabrication of surface modified-PCL nanofibrous scaffolds [52-54].

#### 3.5.3. *In vitro* drug release behavior

The loading and encapsulation efficiencies were found to be the maximum amount of the starting drug concentrations (99 and 98.7%, respectively). This was because the fabrication method did not include any washing or filtration steps that could cause drug loss. The cumulative (%) drug release profiles of indomethacin from the prepared nanofibers scaffolds containing indomethacin (NF4, NF6 and NF7) are represented in Fig. 6. In the beginning, the scaffolds recorded very little drug release (up to 5%) and this was attributed to the instant release of attached drug molecules at the nanofibers surface. There are two different performances of the scaffolds were noted. NF4 scaffold, which is coated with chitosan loaded with indomethacin revealed a relative faster release rate (up to 16%) than the other two scaffolds. While, the other scaffolds (NF6 and NF7) revealed prolonged release behavior (up to 9%) that was attributed to presence of 58S (NF6) or presence of the drug into the nanofibers matrix (NF7). This suggested possible positive effect of 58S on the indomethacin retention within the layer of chitosan (NF6) or presence of the drug into the nanofibers matrix (NF7) that caused sustained drug release in addition to chitosan coating that resulted in controlled drug release [46]. The overall assessments in the PBS are highlighting the positive effect of loading inorganic nanomaterials within the PCL matrix along with surface modifications occurred by chitosan coatings on the drug release, ions exchange and mass loss of the investigated nanofibers scaffolds.

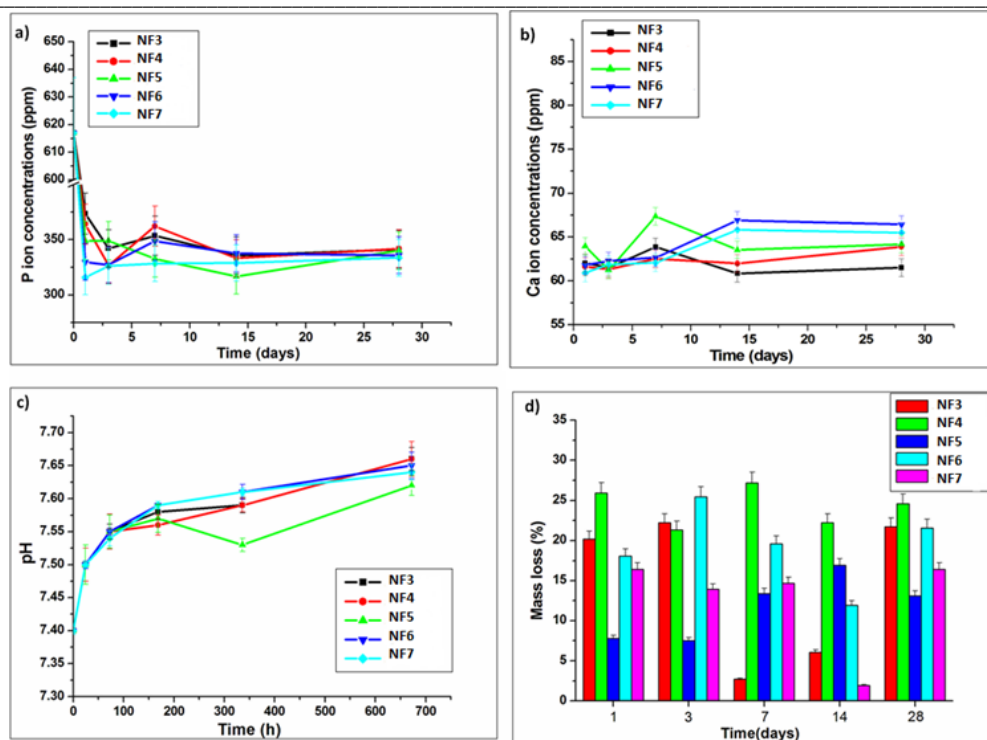


Figure 5. Average ions concentrations of a) P ion, b) Ca ion in the PBS at distinctive time intervals; c) corresponding pH values recorded at the same intervals and d) Mass loss (%)

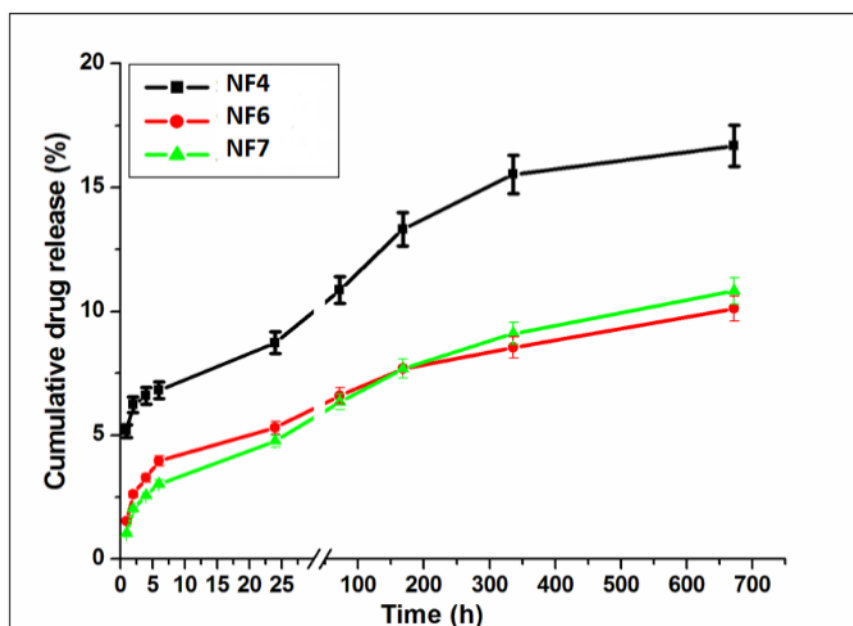


Figure 6. Cumulative drug release (%) of indomethacin from NF4, NF6 and NF7 measured in PBS

### 3.6. Indomethacin kinetic release

The kinetic release of indomethacin throughout the homogenous fibrous scaffolds achieved in this research was evaluated by fitting the release data using the above mentioned mathematical models. The achieved parameters from the fitting process are listed in Table 3. As demonstrated in the previous section, the indomethacin *in vitro* performance from the fabricated scaffolds shows controlled and prolonged behaviors of release in general. It was affirmed that indomethacin kinetic releases follow the Krosmeier-Peppas mathematical model as it possessed higher values of  $R^2$  (0.992, 0.944 and 0.958) compared to zero-order and Fickian diffusion models. In addition, the  $n$  values were lower than 0.5, which indicate that the release mechanism is governed by quasi-Fickian diffusion. The diffusion mechanism from relatively low degradable polymers such as PCL in our case is suggested to be through channels made by PBS solution as early described [37].

**Table 3. Release kinetics parameters of different indomethacin-loaded scaffolds**

Formula code	R <sup>2</sup> -value <sup>†</sup>			Korsmeyer-Peppas model		n	RE <sub>0-672h</sub> <sup>‡</sup> (%)
	Zero-order	Fickian diffusion	Korsmeyer-Peppas model	t <sub>50</sub> <sup>**</sup> (hours)	t <sub>90</sub> <sup>***</sup> (hours)		
NF4	0.776	0.948	0.992	48.929	91.695	0.181	16.675
NF6	0.724	0.902	0.944	91.628	166.414	0.256	10.113
NF7	0.769	0.938	0.958	103.432	187.114	0.325	10.827

**n**: is the diffusion exponent, **t<sub>50</sub><sup>\*\*</sup>**: is time required for 50% of the drug to be released, **t<sub>90</sub><sup>\*\*\*</sup>**: is time required for 90% drug to be released, **‡RE<sub>0-672h</sub>**: is the release efficiency of drug from 0 to 720 hours, **†R<sup>2</sup>-value**: is the value for regression coefficient

### 3.7. In vitro cell studies

#### 3.7.1. Cells attachments

Cell attachment and morphology on selected scaffolds were evaluated after 3 days post cells seeding on the scaffolds' surfaces as represented in Fig. 7. It shows the cells spreading, cells attachment, growth, proliferation, morphology and migration on the surface of the nanofibrous scaffolds and those modified by chitosan. Fig. 7a (NF3 scaffold) had shown multilayers of flat HDPCs cells ingress into the pores of the scaffold along with collagen fibers that made network conjunctions between cells. Existence of minerals was noted in several points, which are organized with fibrillar bundles. These bundles possess a unique banded structure of collagen. Fig. 7b (NF4 scaffold), it is well observed that the surface of the scaffold was covered also by multilayers of spindle HDPCs cells with highly processes which penetrated into pores, along with a network of collagen conjunctions and collagen fibers that had covered the surface of the scaffold. In addition, some minerals were also noted with globular morphology of bone/dentine like minerals. In another area of the surface, there was fibrous network membrane of collagen denoting that this scaffold had good biocompatibility for HDPCs cells. For this scaffold, HDPCs cells maintained spindle shaped, stellar morphology, stretching along the cluster bounded on network membrane of collagen and cells progressed rapidly after 3 days. The mineralization indicated that nano-58S had significantly promoted mineral nodule formation on surface of scaffold was covered by cells, heavy collagen fibers, and minerals. Also, there were many clusters of cells adhered on the scaffold (NF6), the adhesion sites through many bundles of cells (Fig.

7d). There were multilayers of spindle flat HDPCs cells, collagen fibers and biominerals. This scaffold was characterized by an extracellular matrix from the HDPCs cells denoting the inducing significantly higher collagen production compared to other scaffolds. Scaffolds demonstrated an outstanding role in effective regeneration of tissues, including dentin-pulp complex tissues. Dentin progenitor can effectively stimulate cells to consume the 3D micro-environment supported by the scaffolds, including physical roughness and stiffness, chemical composition. Thus, allows cells multiplication and induction into odontogenesis, to the stage required for repair and regeneration process of dentin [55]. The chitosan showed a great proliferation toward bone cell line and this is consistent with other studies [56, 57].

#### 3.7.2. Density of mineralized nodules

The SEM images of the homogenous electrospinning scaffolds after cultured in vitro with dental stem cells for 21 days are represented in Fig. 8. All scaffolds were characterized by presence of calcified collagen fibers and biomineral aggregates on the scaffold's surfaces, along with dental cells infiltrated within pores especially for scaffold (NF5). The surface of scaffold NF5 was covered by thick layer of biominerals which was self-induced with osteogenic induction media and dental cells as compared to the other scaffolds. The presence of mineral nodule formation is phenotype of differentiation. There are obvious of cellular activities processes including great secretions of long fibers of collagen which have covered the surface as matrix with bone/dentine like denoting the formation of mature cells. Some collagen fibers were infiltration through the pores of the prepared scaffold. The density of mineralized nodules secreted by HDPCs cells and the apatite accumulations of calcium and phosphate ions denoting the formation of mature cells. Some collagen fibers were infiltration through the pores of the prepared scaffold. The density of mineralized nodules secreted by HDPCs cells and the accumulation of minerals was significantly higher in scaffolds containing 58S than in the other scaffolds.

Cells are capable to regenerate neo-tissues, if they are supplied with convenient 3D scaffolds that mimic their ECM. Mimicking the features of ECM has subsequently been introduced as a promising process in the dentin scaffold fabrication. Thus, cells favor interacting positively to the ECMs in their attachment, proliferation, differentiation and mineralization processes [58].

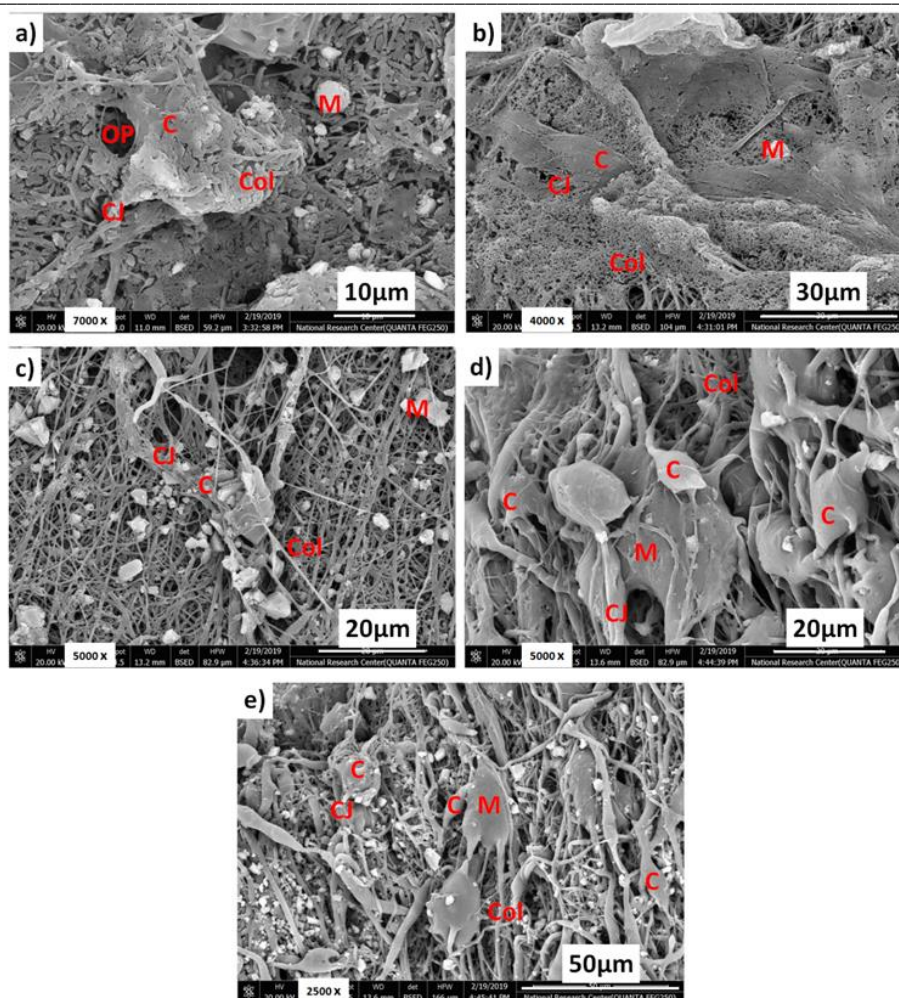


**Figure 7.** SEM images of a) NF3, b) NF4, c) NF5 d) NF6 and e) NF7 after 3 days; OP: open pores, C: Cell, CJ: Cell joints, Col: Collagen, and M: Mineralization

Here in, multilayer scaffolds were obtained by electrospinning for loading dental stem cells. The 58S containing scaffolds and those coated by chitosan possess magnificent physicochemical features along with convenient surface area that played important role in developing more intense collagen fibers and have faster spread and infiltration rates. In addition, differentiation and ECM production were both similar as they recorded a similar occurrence, amounts of collagen, calcium and phosphorous production. However, it is thought that scaffolds contain drug demonstrated relative increase in minerals and intense collagen fibers compared to other scaffolds.

### 3.8. Cytocompatibility of the synthesized materials

#### 3.8.1. Mode of cell death

The mode of cell death is considered as a mark of the cells viability for the under investigated samples in the current research. Figures 9, 10 and 11 showed the cell viabilities of (NF3, NF4, NF5, NF6 and NF7) for two time intervals 24 and 72 h after the exposure to human bone osteosarcoma cell line (MG-63). Images in Fig. 10 shows an increase in the cellular density from 24 to 72 h except for sample NF5, which shows significant apoptotic and necrotic cell death especially at 72 h. Sample NF3 shows apoptotic and necrotic changes in both time intervals especially at 72 h. Sample NF7 demonstrated an increase in cellular density at 72 h but this was accompanied by an increase in apoptotic and necrotic changes as well. From these results, it could be concluded that the best samples are NF4 and NF6, which could be owed to the presence of drug in the coated layer. NF7 comes later after NF4 and NF6 samples because it contains the drug within nanofibers matrix that caused sustained drug release. Finally, samples NF3 and NF5 demonstrated relatively lower viability due to the absence of drug. This was also affirmed by the cell mode of death represented in Fig. 10 that was calculated from the obtained images in Fig. 9. The apoptotic pathway was the predominant one for all the dead cells after being exposed to all the tested samples. The necrotic pathway was obvious only in NF5 (24 and 72 h) and sample NF7 after 72 h.

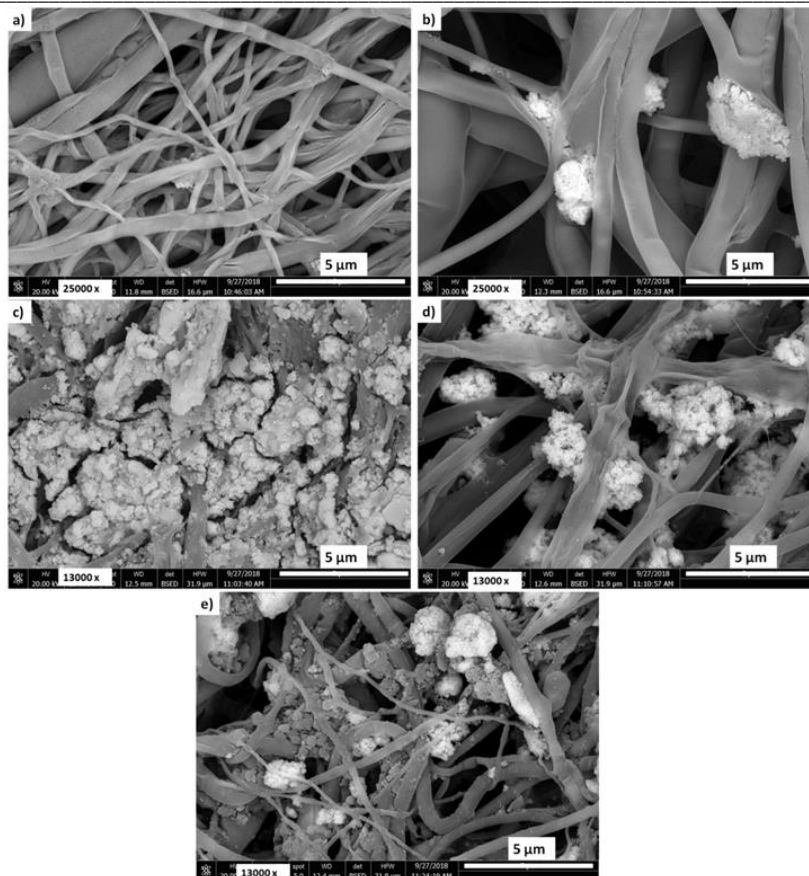


Figure 8. SEM images of a) NF3, b) NF4, c) NF5, d) NF6 and e) NF7 after 21 days

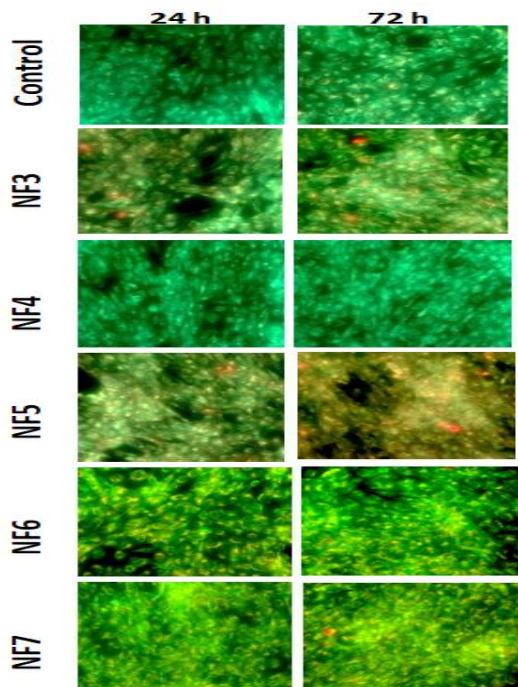


Figure 9. Mode of cell death using acridine orange/ethidium bromide stain on MG-63 cells. The magnification 20X. The scale bar 100 μm.

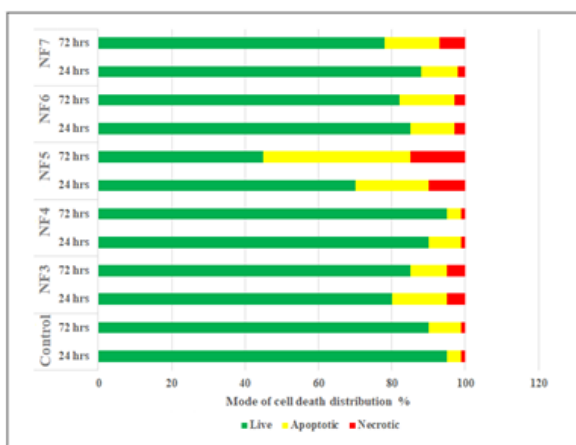


Figure 10. The distribution percentage of the mode of cell death

### 3.8.2. MTT cytotoxicity

Fig. 11 showed the cell proliferation of the different samples on MG-63 cell line after 24 and 72 h. The results revealed there is a significant cell proliferation on time basis for NF3, NF4, and NF7. While, sample NF5 shows significant cytotoxicity after 72 h compared to 24 h. NF6 has no significant difference in cell proliferation between 24 and 72 h. NF4 showed a significant increased proliferation overall all other samples. Also NF7 sample showed significant increased proliferation overall all other samples except NF4. NF3 showed significant increase in proliferation compared to NF5 and NF6. NF6 proliferated significantly over NF5 only. NF5 (contains 58S without the drug), showed a significant cytotoxicity compared to the other samples. Moreover, the cell proliferation demonstrated a significant proliferation for all samples on human bone osteosarcoma cell line (MG-63), which increases the chances of the current developed materials to be implemented in regeneration of damaged bone sites. These results are consistent with some articles that revealed the biocompatibility and proliferation of chitosan [56, 57].

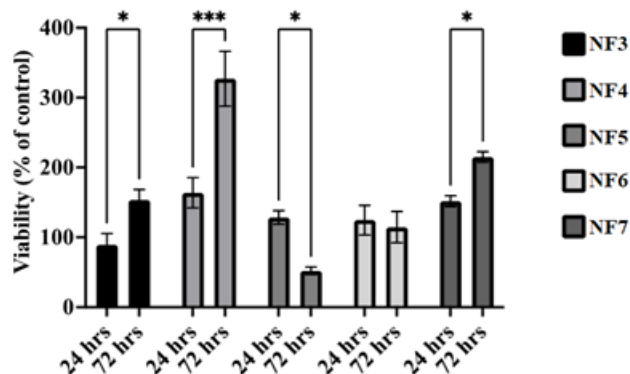


Figure 11. The cell proliferation of different samples exposed to MG-63 cell line after 24 and 72 h. n =3, \* p< 0.05, \*\*\* p< 0.001

### Conclusion

Successful synthesis of homogenous 3D scaffolds utilizing PCL mesh nanofibers loaded with 58S and indomethacin drug to support dental tissue formation was achieved. Alteration of surface activities of PCL scaffolds employing chitosan was affirmed in this research. Microstructure of the created nanocomposite platforms indicated reasonable pore size, surface area and morphology. Indomethacin release and scaffolds degradation were found to be adjusted by the existence of 58S. Cells expansion and development were affirmed by SEM pictures recorded after various testing times. The thickness of mineralized masses produced by HDPPSCs and the aggregation of minerals were essentially higher in platforms containing (58S) than in different scaffolds. Moreover, the cell proliferation demonstrated significant proliferation for the coated nanofibers on human bone osteosarcoma cell line (MG-63). From the obtained results, it was concluded that the presence of 58S and/or indomethacin (NF4 and NF6), enhances the biocompatibility features of the fabricated scaffolds. Hence, in the current article the developed novel 3D homogeneous scaffolds are suggested to implementation in controlled delivery of indomethacin and dental tissue recovery.

### Statements and Declarations

#### Ethical Approval

The *in vitro* assessments using the primary Human dental pulp stem cells (HDPPSCs) were approved by the Medical Research Ethics Committee (MREC) of National Research Centre (NRC), Egypt (Approval No.: 16/340). The utilized cells were supplied by the Holding Company for Biological Products & Vaccines (VACSERA), Cairo, Egypt. The cytocompatibility of the synthesized materials using the Human bone osteosarcoma (MG-63) was approved by the Medical Research Ethics Committee (MREC) of National Research Centre (NRC), Egypt (Approval No.: 095082023). Federal Wide Assurance No.: FWA 00014747.

#### Competing interests

The authors declare that there is no conflict of interests regarding the publication of this paper.

#### Authors' contributions

All authors have equally contributed to the following tasks, made co-design of experimental set-up and conduct of all experiments; generation and preparation of results for publishing; interpretation of results; preparation of original draft; joint preparation of the subsequent drafts. In addition, they have conceptualized the study; funding arrangement; editing and correction of all drafts.

### Availability of data and materials

The data and materials are available upon request.

### References

- [1]. Kumar, T. S. M., Kumar, K. S., Rajini, N., Siengchin, S., Ayrilmis, N., & Rajulu, A. V. A comprehensive review of electrospun nanofibers: Food and packaging perspective. *Composites Part B: Engineering*. **175**, 107074 (2019).
- [2]. Cao, S., Zhao, Y., Hu, Y., Zou, L., & Chen, J. New perspectives: In situ tissue engineering for bone repair scaffold. *Composites Part B: Engineering*. **202**, 108445 (2020).
- [3]. Bekas, D. G., Tsirka, K., Baltzis, D., & Paipetis, A. S. Self healing materials: A review of advances in materials, evaluation, characterization and monitoring techniques. *Composites Part B: Engineering* **87**, 92–119 (2016).
- [4]. Chung, D. D. L. A review of multifunctional polymer matrix structural composites. *Composites Part B: Engineering* **160**, 644–660 (2019).
- [5]. Mabrouk, M., Beherei, H. H., & Das, D. B. Recent progress in the fabrication techniques of 3D scaffolds for tissue engineering. *Materials Science and Engineering C*. **110**, 110716 (2020).
- [6]. Kahdim, O. S., Abdelmoula, N., Al Karagoly, H., Albukhaty, S., & Al Saaidi, J. Fabrication of a polycaprolactone/Chitosan nanofibrous scaffold loaded with nigella sativa extract for biomedical applications. *BioTech* **12**(1), 19 (2023).
- [7]. Abukhaty, S., Al Karagoly, H., Allafchian, A. R., Jalali, S. A. H., Al Kelabi, T., & Muhannad, M. Production and characterization of biocompatible nanofibrous scaffolds made of  $\beta$  sitosterol loaded polyvinyl alcohol/tragacanth gum composites. *Nanotechnology* **33**(8), 085102 (2021).
- [8]. Song, J., Gao, H., Zhu, G., Cao, X., Shi, X., & Wang, Y. The preparation and characterization of polycaprolactone/graphene oxide biocomposite nanofiber scaffolds and their application for directing cell behaviors. *Carbon*. **95**, 1039–1050 (2015).
- [9]. Safari, B., Aghanejad, A., Roshangar, L., & Davaran, S. Osteogenic effects of the bioactive small molecules and minerals in the scaffold based bone tissue engineering. *Colloids and Surfaces B: Biointerfaces*. **198**, 111462 (2021).
- [10]. Rezvani, Z., Venugopal, J. R., Urbanska, A. M., Mills, D. K., Ramakrishna, S., & Mozafari, M. A bird's eye view on the use of electrospun nanofibrous scaffolds for bone tissue engineering: Current state-of-the-art, emerging directions and future trends. *Nanomedicine: Nanotechnology, Biology and Medicine* **12**(7), 2181–2200 (2016).
- [11]. Cai, Y. Z., Zhang, G. R., Wang, L. L., Jiang, Y. Z., Ouyang, H. W., & Zou, X. H. Novel biodegradable three-dimensional macroporous scaffold using aligned electrospun nanofibrous yarns for bone tissue engineering. *Journal of Biomedical Materials Research Part A* **100**(5), 1187–1194 (2012).
- [12]. Wang, W., Itoh, S., Konno, K., Kikkawa, T., Ichinose, S., Sakai, K., ... & Watabe, K. Effects of Schwann cell alignment along the oriented electrospun chitosan nanofibers on nerve regeneration. *Journal of Biomedical Materials Research Part A*. **91**(4), 994–1005 (2009).
- [13]. Steffens, D., Braghirolli, D. I., Maurmann, N., & Pranke, P. Update on the main use of biomaterials and techniques associated with tissue engineering. *Drug discovery today* **23**(8), 1474–1488 (2018).
- [14]. Choi, E., Bae, S., Kim, D., Yang, G. H., Lee, K., You, H. J., ... & Jeon, H. Characterization and intracellular mechanism of electrospun poly( $\epsilon$  caprolactone)(PCL) fibers incorporated with bone dECM powder as a potential membrane for guided bone regeneration. *Journal of Industrial and Engineering Chemistry* **94**, 282–291 (2021).
- [15]. Badrossamav, M. R., McIlwee, H. A., Goss, J. A., & Parker, K. K. Nanofiber assembly by rotary jet spinning. *Nano letters* **10**(6), 2257–2261(2010).
- [16]. Zhang, D., & Chang, J. Electrospinning of three dimensional nanofibrous tubes with controllable architectures. *Nano letters*. **8**(10), 3283–3287 (2008).
- [17]. Yan, G., Yu, J., Qiu, Y., Yi, X., Lu, J., Zhou, X., & Bai, X. Self assembly of electrospun polymer nanofibers: A general phenomenon generating honeycomb patterned nanofibrous structures. *Langmuir*. **27**(8), 4285–4289 (2011).
- [18]. He, B., Ou, Y., Chen, S., Zhao, W., Zhou, A., Zhao, J., ... & Zhu, Y. Designer bFGF incorporated d form self assembly peptide nanofiber scaffolds to promote bone repair. *Materials Science and Engineering: C* **74**, 451–458 (2017).
- [19]. Abdelaziz, A. G., Nageh, H., Abdo, S. M., Abdalla, M. S., Amer, A. A., Abdal Hay, A., & Barhoum, A. A Review of 3D Polymeric Scaffolds for Bone Tissue Engineering: Principles, Fabrication Techniques, Immunomodulatory Roles, and Challenges. *Bioengineering* **10**(2), 204 (2023).
- [20]. Sun, B., Long, Y. Z., Yu, F., Li, M. M., Zhang, H. D., Li, W. J., & Xu, T. X. Self assembly of a three dimensional fibrous polymer sponge by electrospinning. *Nanoscale* **4**(6), 2134–2137 (2012).
- [21]. Sun, B., Long, Y. Z., Zhang, H. D., Li, M. M., Duvail, J. L., Jiang, X. Y., & Yin, H. L. Advances in three dimensional nanofibrous macrostructures via electrospinning. *Progress in Polymer Science*. **39**(5), 862–890 (2014).
- [22]. Leung, L. H., Fan, S., & Naguib, H. E. Fabrication of 3D electrospun structures from poly (lactide-co-glycolide acid) nano-hydroxyapatite composites. *Journal of Polymer Science Part B: Polymer Physics*. **50**(4), 242–249 (2012).
- [23]. Teo, W. E., Inai, R., & Ramakrishna, S. Technological advances in electrospinning of nanofibers. *Science and technology of advanced materials* (2011).

- [24]. Chandika, P., Heo, S. Y., Kim, T. H., Oh, G. W., Kim, G. H., Kim, M. S., & Jung, W. K. Recent advances in biological macromolecule based tissue-engineered composite scaffolds for cardiac tissue regeneration applications. *International Journal of Biological Macromolecules*. **164**, 2329-2357 (2020).
- [25]. Jin, L., Feng, Z. Q., Wang, T., Ren, Z., Ma, S., Wu, J., & Sun, D. A novel fluffy hydroxylapatite fiber scaffold with deep interconnected pores designed for three-dimensional cell culture. *Journal of Materials Chemistry B*. **2**(1), 129-136 (2014).
- [26]. Beherei, H. H., Shaltout, A. A., Mabrouk, M., Abdelwahed, N. A., & Das, D. B. Influence of niobium pentoxide particulates on the properties of brushite/gelatin/alginate membranes. *Journal of Pharmaceutical Sciences*. **107**(5), 1361-1371 (2018).
- [27]. Tohamy, K. M., Mabrouk, M., Soliman, I. E., Beherei, H. H., & Aboelnasr, M. A. Novel alginate/hydroxyethyl cellulose/hydroxyapatite composite scaffold for bone regeneration: In vitro cell viability and proliferation of human mesenchymal stem cells. *International Journal of Biological Macromolecules*. **112**, 448-460 (2018).
- [28]. El-Meliegy, E., Mabrouk, M., Kamal, G. M., Awad, S. M., El-Tohamy, A. M., & El Gohary, M. I. Anticancer drug carriers using dicalcium phosphate/dextran/CMCnanocomposite scaffolds. *Journal of Drug Delivery Science and Technology*. **45**, 315-322 (2018).
- [29]. Wang, Y., Zhu, G., Li, N., Song, J., Wang, L., & Shi, X. Small molecules and their controlled release that induce the osteogenic/chondrogenic commitment of stem cells. *Biotechnology advances*. **33**(8), 1626-1640 (2015).
- [30]. Ng, I. S., Ooi, C. W., Liu, B. L., Peng, C. T., Chiu, C. Y., & Chang, Y. K. Antibacterial efficacy of chitosan-and poly (hexamethylene biguanide)-immobilized nanofiber membrane. *International journal of biological macromolecules*. **154**, 844-854 (2020).
- [31]. Surgutskaia, N. S., Di Martino, A., Zednik, J., Ozaltin, K., Lovecká, L., Bergerova, E. D., ... & Sedlarik, V. Efficient Cu<sup>2+</sup>, Pb<sup>2+</sup> and Ni<sup>2+</sup> ion removal from wastewater using electrospun DTPA-modified chitosan/polyethylene oxide nanofibers. *Separation and Purification Technology*. **247**, 11691 (2020).
- [32]. Al-Musawi, M. H., Rashidi, M., Mohammadzadeh, V., Albukhaty, S., Mahmoudi, E., & Ghorbani, M. Development of a novel scaffold based on basil seed gum/chitosan hydrogel containing quercetin-loaded zein microsphere for bone tissue engineering. *Journal of Polymers and the Environment*. **31**(11), 4738-4751 (2023).
- [33]. Govender, M., Indermun, S., Kumar, P., Choonara, Y. E., & Pillay, V. 3D Printed, PVA-PAA Hydrogel Loaded-Polycaprolactone Scaffold for the Delivery of Hydrophilic In-Situ Formed Sodium Indomethacin. *Materials*. **11**(6), 1006 (2018).
- [34]. Guo, Y. C., Chang, C. M., Hsu, W. L., Chiu, S. J., Tsai, Y. T., Chou, Y. H., ... & Chang, W. C. Indomethacin inhibits cancer cell migration via attenuation of cellular calcium mobilization. *Molecules*. **18**(6), 6584-6596 (2013).
- [35]. Taha, E. I. Development and characterization of new indomethacin self-nanoemulsifying formulations. *Scientia Pharmaceutica*. **77**(2), 443-452 (2009).
- [36]. Morsy, R. A., Beherei, H., Ellithy, M., Tarek, H. E., & Mabrouk, M. The odontogenic performance of human dental pulp stem cell in 3-dimensional chitosan and nano-bioactive glass-based scaffold material with different pores size. *Journal of The Arab Society for Medical Research*. **14**(2), 82-94 (2019).
- [37]. Mabrouk, M., Beherei, H. H., ElShebiney, S., & Tanaka, M. Newly developed controlled release subcutaneous formulation for tramadol hydrochloride. *Saudi pharmaceutical journal*. **26**(4), 585-592 (2018).
- [38]. Matsiko, A., Gleeson, J. P., & O'Brien, F. J. Scaffold mean pore size influences mesenchymal stem cell chondrogenic differentiation and matrix deposition. *Tissue Engineering Part A*. **21**(3-4), 486-497 (2015).
- [39]. Leite, M., Quinta-Costa, M., Leite, P. S., & Guimarães, J. E. Critical evaluation of techniques to detect and measure cell death—study in a model of UV radiation of the leukaemic cell line HL60. *Analytical Cellular Pathology*. **19**, 139-151 (1999).
- [40]. Hansen, M. B., Nielsen, S. E., & Berg, K. Re-examination and further development of a precise and rapid dye method for measuring cell growth/cell kill. *Journal of immunological methods*. **119**(2), 203-210 (1989).
- [41]. Mabrouk, M., Bijjukumar, D., Mulla, J. A., Chejara, D. R., Badhe, R. V., Choonara, Y. E., ... & Pillay, V. Enhancement of the biomineralization and cellular adhesivity of polycaprolactone-based hollow porous microspheres via dopamine bio-activation for tissue engineering applications. *Materials Letters*. **161**, 503-507 (2015).
- [42]. Lee, Y. B., Song, S. J., Shin, Y. C., Jung, Y. J., Kim, B., Kang, M. S., ... & Han, D. W. Ternary nanofiber matrices composed of PCL/black phosphorus/collagen to enhance osteodifferentiation. *Journal of Industrial and Engineering Chemistry*. **80**, 802-810 (2019).
- [43]. Song, J., Zhu, G., Wang, L., An, G., Shi, X., & Wang, Y. Assembling of electrospun meshes into three-dimensional porous scaffolds for bone repair. *Biofabrication*. **9**(1), 015018 (2017).
- [44]. Shoja, M., Shameli, K., Ahmad, M. B., & Zakaria, Z. Preparation and characterization of Poly ( $\epsilon$ -Caprolactone)/TiO<sub>2</sub> micro-composites. *Digest Journal of Nanomaterials and Biostructures*. **10**(2), 471-477 (2015).
- [45]. El-Meliegy, E., Mabrouk, M., El-Sayed, S. A., Abd El-Hady, B. M., Shehata, M. R., & Hosny, W. M. Novel Fe<sub>2</sub>O<sub>3</sub>-doped glass/chitosan scaffolds for bone tissue replacement. *Ceramics International*. **44**(8), 9140-9151 (2018).
- [46]. Nikonenko, N. A., Buslov, D. K., Sushko, N. I., & Zhabankov, R. G. Investigation of stretching vibrations of glycosidic linkages in disaccharides and polysaccharides with use of IR spectra deconvolution. *Biopolymers: Original Research on Biomolecules*. **57**(4), 257-262 (2000).
- [47]. Huang, B. C., Yi, Y. C., Chang, J. S., & Ng, I. S. Mechanism study of photo-induced gold nanoparticles formation by *Shewanella oneidensis* MR-1. *Scientific reports*. **9**(1), 7589 (2019).

- [48]. Luo, W., Bai, Z., & Zhu, Y. Fast removal of Co (ii) from aqueous solution using porous carboxymethyl chitosan beads and its adsorption mechanism. *RSC advances*. **8**(24), 13370-13387 (2018).
- [49]. Mondésert, H., Bossard, F., & Favier, D. Anisotropic electrospun honeycomb polycaprolactone scaffolds: Elaboration, morphological and mechanical properties. *Journal of the mechanical behavior of biomedical materials*. **113**, 104124 (2021).
- [50]. Kundu, K., Afshar, A., Katti, D. R., Edirisinghe, M., & Katti, K. S. Composite nanoclay-hydroxyapatite-polymer fiber scaffolds for bone tissue engineering manufactured using pressurized gyration. *Composites Science and Technology*. **202**, 108598 (2021).
- [51]. Kumari, S., Tiyyagura, H. R., Pottathara, Y. B., Sadasivuni, K. K., Ponnamma, D., Douglas, T. E., ... & Mohan, M. K. Surface functionalization of chitosan as a coating material for orthopaedic applications: A comprehensive review. *Carbohydrate polymers*. **255**, 117487 (2021).
- [52]. Goudarzi, Z. M., Behzad, T., Ghasemi-Mobarakeh, L., & Kharaziha, M. An investigation into influence of acetylated cellulose nanofibers on properties of PCL/Gelatin electrospun nanofibrous scaffold for soft tissue engineering. *Polymer*. **213**, 123313 (2021).
- [53]. Fadaie, M., Mirzaei, E., Geramizadeh, B., & Asvar, Z. Incorporation of nanofibrillated chitosan into electrospun PCL nanofibers makes scaffolds with enhanced mechanical and biological properties. *Carbohydrate polymers*. **199**, 628-640 (2018).
- [54]. Ghaee, A., Bagheri-Khoulenjani, S., Afshar, H. A., & Bogheiri, H. Biomimetic nanocomposite scaffolds based on surface modified PCL-nanofibers containing curcumin embedded in chitosan/gelatin for skin regeneration. *Composites Part B: Engineering*. **177**, 107339 (2019).
- [55]. Jennings, J. A., Wells, C. M., McGraw, G. S., Velasquez Pulgarin, D. A., Whitaker, M. D., Pruitt, R. L., & Bumgardner, J. D. Chitosan coatings to control release and target tissues for therapeutic delivery. *Therapeutic Delivery*. **6**(7), 855-871(2015).
- [56]. Doderò, A., Scarfi, S., Mirata, S., Sionkowska, A., Vicini, S., Alloisio, M., & Castellano, M. Effect of crosslinking type on the physical-chemical properties and biocompatibility of chitosan-based electrospun membranes. *Polymers*. **13**(5), 831 (2021).
- [57]. Fletes-Vargas, G., Espinosa-Andrews, H., Cervantes-Uc, J. M., Limón-Rocha, I., Luna-Bárcenas, G., Vázquez-Lepe, M., ... & Rodríguez-Rodríguez, R. Porous chitosan hydrogels produced by physical crosslinking: physicochemical, structural, and cytotoxic properties. *Polymers*. **15**(9), (2023).
- [58]. Nam, S., Won, J. E., Kim, C. H., & Kim, H. W. Odontogenic differentiation of human dental pulp stem cells stimulated by the calcium phosphate porous granules. *Journal of tissue engineering*. (2011).